A comparison of diagnostics for AMOC heat transport applied to the CESM large ensemble

C Spencer Jones¹, Scout Jiang² and Ryan P. Abernathey²

- ¹Texas A&M University, College Station, TX
- ²Columbia University, New York, NY

Key Points:

- We compare four diagnostics for AMOC heat transport that partition the flow into mass-conserving gyre and overturning components
 - A new physically-motivated method is compared with the standard method that relies on zonally averaging the temperature and velocity fields
- All four methods yield different estimates of the fraction of time-mean heat transport performed by AMOC

Corresponding author: C. Spencer Jones, spencerjones@tamu.edu

Abstract

13

31

32

33

34

35

37

38

30

40

41

42

43

Atlantic time-mean heat transport is northward at all latitudes and exhibits strong mul-14 tidecadal variability between about 30°N and 55°N. Atlantic heat transport variability 15 influences many aspects of the climate system, including regional surface temperatures, 16 subpolar heat content, Arctic sea-ice concentration and tropical precipitation patterns. 17 Atlantic heat transport and heat transport variability are commonly partitioned into two 18 components: the heat transport by the AMOC and the heat transport by the gyres. In 19 this paper we compare four different methods for performing this partition, and we ap-20 ply these methods to the CESM1 Large Ensemble at 34°N, 26°N and 5°S. We discuss 21 the strengths and weaknesses of each method. The four methods all give significantly 22 different estimates for the proportion of the time-mean heat transport performed by AMOC. 23 One of these methods is a new physically-motivated method based on the pathway of 24 the northward-flowing part of AMOC. This paper presents a preliminary version of our 25 method that works only when the AMOC follows the western boundary of the basin. All 26 the methods agree that at 26°N, 80-100% of heat transport variability at 2-10yr timescales 27 is performed by AMOC, but there is more disagreement between methods in attribut-28 ing multidecadal variability, with some methods showing a compensation between the 29 AMOC and gyre heat transport variability. 30

Plain Language Summary

Scientists often want to quantify how much heat is transported by the Atlantic Meridional Overturning Circulation (sometimes called the "Conveyor Belt" circulation) and how much heat is transported by the ocean's gyres. This paper compares some different methods for estimating the heat transport by the overturning circulation and by the gyres, including a new method that has not been used before. There are significant differences in the results of each method, and here we discuss the strengths and weaknesses of each method.

1 Introduction

The Atlantic Meridional Overturning Circulation (AMOC) comprises northward flow of warmer water near the surface, deep water formation in the North Atlantic, and southward flow of cooler water at depth. The AMOC transports heat northward throughout the Atlantic basin, warming the Northern Hemisphere (Jackson et al., 2015; Buckley & Marshall, 2016) and performing 20% of the total planetary poleward heat transport at 26.5°N (Trenberth & Fasullo, 2017). The AMOC's cross-equatorial heat transport shifts the intertropical convergence zone (ITCZ) northward, affecting precipitation
patterns close to the equator (Kang et al., 2009; Marshall et al., 2014).

Variations in northward Atlantic heat transport are thought to be a key driver of Atlantic Multideadal Variability (Oldenburg et al., 2021), which affects variability in multiple parts of the climate system (Zhang et al., 2019), including tropical precipitation (Folland et al., 1986; Martin & Thorncroft, 2014), Atlantic hurricane frequency (Goldenberg et al., 2001; Klotzbach et al., 2015), and North Atlantic sea ice variability (Yeager et al., 2015). Low frequency ocean variability is a source of predictability in the climate system, meaning that parts of the climate system that are driven by AMOC variability may be predictable using observations of the ocean (Borchert et al., 2018). AMOC low-frequency variability and Atlantic decadal predictability vary significantly between climate models (Yan et al., 2018). To understand the cause of differences between models, it is helpful to characterize how the AMOC and the gyres interact to influence northward ocean heat transport. In this paper, we use four different methods to estimate how much ocean heat transport is performed by AMOC.

Many studies have attempted to separate the heat transport by the overturning circulation from the heat transport by the gyres (e.g. Bryan (1962); Hall and Bryden (1982); McDonagh et al. (2010); Ferrari and Ferreira (2011); Piecuch et al. (2017)). The AMOC appears to be the primary driver of heat transport in the subtropical gyre region and that the gyre is a more important driver in the subpolar gyre region (Eden & Willebrand, 2001; Piecuch et al., 2017).

Many of the studies that have partitioned the heat transport by the gyres and the heat transport by the overturning circulation have done so with the goal of identifying how much of the heat transport variability is driven by wind and how much is driven by buoyancy forcing. AMOC variability is often thought to be primarily driven by buoyancy forcing, and the gyres are thought to be primarily driven by wind forcing. But recent studies have shown that gyre strength is strongly influenced by buoyancy forcing (Bhagtani et al., 2023), and that AMOC strength is strongly influenced by wind forcing (J. Yang, 2015; Cessi, 2018). The goal of this study is not to partition the heat transport caused by wind from the heat transport caused by buoyancy forcing, but to eluci-

date how the total AMOC transport influences heat transport at multiple latitudes, and to look at how different methods for finding the heat transport by the AMOC perform differently.

Most previous studies define the heat transport by the overturning as the zonal integral of the volume transport multiplied by the zonal mean temperature, integrated in the vertical. In all the studies that use this method, the integrals are taken in depth space. In the last twenty years or so, oceanographers have started to define the AMOC using a zonal-average in density space (Foukal & Chafik, 2022). Recent work by Zhang and Thomas (2021) has shown that flows on the same depth level in the subpolar gyre region have different densities and form part of the AMOC. It is clear that the old depth-averaged way of looking at things can still be useful, but much progress has been made by looking at the AMOC in new ways. In this work, we compare the zonal-mean method described in most previous studies, in which the mean is taken along depth surfaces, with a similar method in which the mean is taken along density surfaces.

Northward flow in the subtropical North Atlantic is dominated by the Gulf Stream. The Gulf Stream is significantly stronger than required to return the Sverdrup transport (Gray & Riser, 2014), which can partly be attributed to the presence of an additional flow component: the northward component of the AMOC. In the absence of mixing or surface forcing, water flows along isopycnals, so lighter Gulf Stream waters are less likely to continue northward into the subpolar gyre. Talley (2003) proposed a method for dividing the ocean heat transport into heat transport by the overturning and heat transport by the gyres by assigning lighter Gulf Stream waters to the subtropical gyre and denser waters to the AMOC. Recent work by Berglund et al. (2022) shows that denser waters are more likely to continue northward into the subpolar gyre, sugesting that the Talley (2003) method is based on correct physical assumptions. In this manuscript, we compare the Talley (2003) method with the other methods discussed above.

Northward AMOC transport primarily follows the western boundary at latitudes where the gyre is clockwise (Stommel, 1957). Rypina et al. (2011) showed that drifters in the far west of the Gulf Stream are likely to reach the North Atlantic, whereas drifters further to the east are unlikely to cross northward into latitudes associated with the subpolar gyre. Hence, an alternative way to divide the AMOC heat transport from the gyre heat transport is to assume the AMOC flow occupies the westernmost portion of the basin

at latitudes with a clockwise gyre. In this work we apply this approach to create a new method for partitioning ocean heat transport.

This new method is also conceptually similar to a method used by Roemmich and Wunsch (1985). Roemmich and Wunsch (1985) estimated the temperature transport in the deep ocean, the temperature transport in the western boundary current, and the temperature transport in the southward flowing part of the gyre from observations. Talley (1999) used a similar method. These authors took the mean temperature in the western boundary current and calculated the heat transport by the AMOC to be the volume transport of the AMOC multiplied the difference in temperature between the western boundary current and the deep ocean. Roemmich and Wunsch (1985) applied their method to sections at 24°N and found that 90% of the mean northward heat transport is performed by the AMOC at this latitude, and they commented that the northward heat transport is dominated by the AMOC across multiple years of observations.

In this work, we compare all four of the above methods for partitioning ocean heat transport into heat transport by the overturning and heat transport by the gyres. We use the CESM large ensemble as a testbed for these different methods, because the existence of long runs and many ensemble members allows us to examine variability at multiple timescales. The CESM large ensemble is described in section 2 and the four methods for partitioning heat transport by the overturning and heat transport by the gyres are described in section 2.1. Section 3.1 shows the results of different methods for partitioning the time-mean heat transport by the overturning and the heat transport by the gyres. Sections 3.2 and 3.3 describe the heat transport variability in the CESM large ensemble, and use the methods to attribute this heat transport variability to the overturning and the gyres. Section 4 discusses the results and presents conclusions.

2 Methods

We explore these diagnostics in the context of ocean models, where the time varying circulation and temperature fields are perfectly known. Our analysis uses a large ensemble of ocean simulations in order to sample broadly the modes of natural variability of the North Atlantic circulation. The CESM Large Ensemble is a group of simulations performed using a 1° nominal resolution fully-coupled version of the Community Earth System Model (CESM1) (Kay et al., 2015). Forty ensemble members were cre-

ated for the period 1920-2100. Each ensemble member has the same radiative forcing scenario, but the initial atmospheric temperature is perturbed with a spatially random perturbation order 10^{-14} K. As a result of internal variability, each ensemble member's state follows a unique trajectory with different regional temperature patterns and different AMOC variability.

We used the cloud-optimized dataset, which is stored on Amazon Web Services (AWS) thanks to the AWS Public Dataset Program (de La Beaujardiere et al., 2019). In this work we used the first 35 ensemble members for the period 1940-2005. 1940 is chosen because this allows time for the internal variability of the system to diverge, so that the ensemble members are different from each other throughout the chosen period. 2005 is a natural end date, because it marks the end of the historical runs for the CESM1 Large Ensemble. During the period 1940-2005 multidecadal variability dominates over long-term trends in AMOC and heat transport. Members of the CESM large ensemble are not meant to have exactly the same variability as the real world, but to represent the range of possible internal variability. Many of the ensemble members exhibit North Atlantic subpolar gyre ocean heat content variability with similar magnitude to ECCOv4r3 (not shown).

2.1 Separating heat transport by the gyre from heat transport by the overturning circulation

Heat transport by the ocean's gyre is primarily wind driven, and the variability of this heat transport is likely to have short time scales and spatial effects that are confined to each gyre. Heat transport by the overturning is both wind and buoyancy driven, and AMOC heat transport variability is more likely to impact temperatures in the far North Atlantic. Hence, it is desirable to partition the heat transport and heat transport variability across a particular latitude into the heat transport by the overturning and the heat transport by the gyres. All the methods described in this section are designed to be applied at a fixed latitude. The notion of heat transport by the flow across a section is only well-defined when the net mass transport (or volume transport, in a Boussinesq ocean model) of the flow is zero (see e.g. Warren (1999); Boccaletti et al. (2005); Pickart and Spall (2007); H. Yang et al. (2015)). In the Atlantic basin, there is a net southward volume transport of about 1 Sv, and the heat transported by this net throughflow is dependent on our choice of reference temperature. Before performing any further subdi-

visions, we remove the net throughflow component of the heat transport. Because the net throughflow is small, the results of this study are relatively insensitive to the choice of reference temperature associated with this throughflow.

At each latitude, we remove the mean velocity from the total velocity to find the volume conserving part of the velocity,

$$v_{vc}(x,z,t) = v(x,z,t) - \overline{v}(t), \qquad (1)$$

where

$$\overline{v}(t) = \frac{\int_{-H}^{0} \int_{x_{w}}^{x_{e}} v(x, z, t) \, dx \, dz}{\int_{-H}^{0} \int_{x_{w}}^{x_{e}} \, dx \, dz},$$
(2)

and x is distance in the longitudinal direction, z is distance in the vertical, v is the meridional velocity, H is the ocean depth, x_w is the western boundary of the Atlantic and x_e is the eastern boundary of the Atlantic. Ideally, the residual velocity (including the eddy transport) would be used in these calculations, but this data was not readily available, so the effects of parameterized eddies are not included in v. We also remove the southward heat transport that is associated with the mean velocity, so the volume conserving part of the ocean heat transport is

$$OHT_{vc}(t) = \int_{-H}^{0} \int_{x_{vv}}^{x_{e}} v(x, z, t) \theta(x, z, t) dx dz - \int_{-H}^{0} \int_{x_{vv}}^{x_{e}} \theta(x, z, t) \overline{v}(t) dx dz,$$
 (3)

where θ is potential temperature referenced to the surface.

The total volume conserving advective heat transport, OHT_{vc} , can be further decomposed into the sum of heat transport by multiple sub-flows, provided that each sub-flow has no net mass transport associated with it. There are infinitely many possible such decompositions. Once the net velocity and associated heat transport have been removed, we apply and compare four methods for separating the heat transport by the overturning and the heat transport by the gyres. These methods are illustrated in figure 1.

2.1.1 Zonal-mean method in z-space

The first method, which we call the zonal-mean method in z-space, has been in use for a long time (Bryan, 1962; Hall & Bryden, 1982; McDonagh et al., 2010; Piecuch et al., 2017). In this method the heat transport by the overturning, $OHT_{ot}^{(z)}(t)$, is calculated by multiplying the zonally-integrated velocity by the zonal-mean temperature, where all the zonal integrals are taken at constant depth, and then integrating in the vertical,

97 SO

204

205

206

207

208

209

210

212

213

214

215

216

217

218

220

$$OHT_{ot}^{(z)}(t) = \int_{-H}^{0} \left(\int_{x_w}^{x_e} v_{vc}(x, z, t) \, dx \right) \left(\frac{\int_{x_w}^{x_e} \theta(x, z, t) \, dx}{\int_{x_w}^{x_e} dx} \right) \, dz \,, \tag{4}$$

as illustrated in the top panel to figure 1. In this method, the heat transport by the gyre is the total volume-conserving heat transport minus the heat transport by the overturning,

$$OHT_{gyre}^{(z)}(t) = OHT_{vc}(t) - OHT_{ot}^{(z)}(t),$$
(5)

where $OHT_{ot}^{(z)}(t)$ is the heat transport attributed to the AMOC by the zonal-mean method in z-space and $OHT_{gyre}^{(z)}(t)$ is the heat transport attributed to the gyre by the zonal-mean method in z-space.

2.1.2 Zonal-mean method in density space

The second method we investigate is similar to the first method, but zonal integrals are taken in density coordinates instead of depth coordinates. Thickness-weighting is necessary to preserve volume conservation (see e.g. Young (2012)), so

$$\begin{aligned}
OHT_{ot}^{(\rho)}(t) &= \int_{\rho_{min}}^{\rho_{max}} \left(\int_{x_w}^{x_e} v_{vc}(x, \rho, t) \zeta_{\tilde{\rho}}(x, \rho, t) dx \right) \left(\frac{\int_{x_w}^{x_e} \theta(x, \rho, t) \zeta_{\tilde{\rho}}(x, \rho, t) dx}{\int_{x_w}^{x_e} \zeta_{\tilde{\rho}}(x, \rho, t) dx} \right) d\rho (6) \\
&\approx \sum_{\rho} \left(\int_{x_w}^{x_e} v_{vc}(x, \rho, t) \delta z(x, \rho, t) dx \right) \left(\frac{\int_{x_w}^{x_e} \theta(x, \rho, t) \delta z(x, \rho, t) dx}{\int_{x_w}^{x_e} \delta z(x, \rho, t) dx} \right), \quad (7)
\end{aligned}$$

where ζ is the depth of a density surface and $\zeta_{\tilde{\rho}}$ is the derivative of ζ with respect to density. When this calculation is discretized, a finite layer thickness δz is used to describe the vertical distance between two isopycnals, and we sum over all densities. This method is illustrated in the second panel of figure 1. As in the first method, the heat transport by the gyre is the total volume-conserving heat transport minus the heat transport by the overturning,

$$OHT_{gyre}^{(\rho)}(t) = OHT_{vc}(t) - OHT_{ot}^{(\rho)}(t), \qquad (8)$$

where $\mathrm{OHT}_{ot}^{(\rho)}(t)$ is the heat transport attributed to the AMOC by the zonal-mean method in density-space and $\mathrm{OHT}_{gyre}^{(\rho)}(t)$ is the heat transport attributed to the gyre by the zonal-mean method in density-space.

It is easy to imagine scenarios in which the above methods will perform badly. For example, as illustrated in the top panel of figure 2, in a scenario with no gyre the zonal mean method in z-space attributes heat transport to the gyre if the zonal mean temperature associated with the northward flow is lower than the temperature of the water that

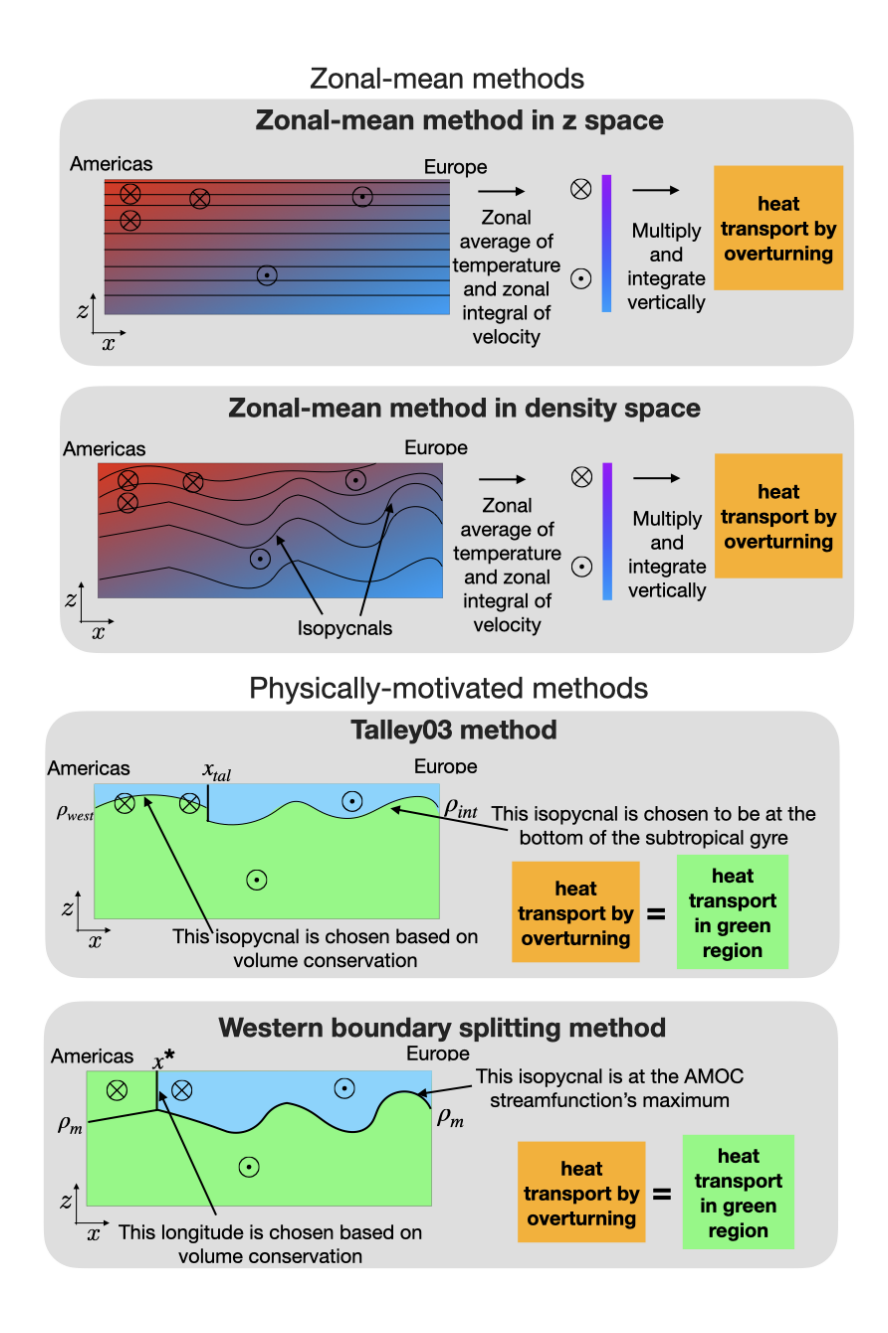


Figure 1. Schematic of four different methods for separating heat transport due to the overturning and heat transport due to the gyre. Note that it only makes sense to apply the Talley03 method in the Northern Hemisphere subtropical gyre, where it is likely that AMOC waters tend to follow the western boundary and to be denser than gyre waters. The version of the Talley03 method used in this paper includes any Ekman transport as part of the gyre.

is flowing northward. It is also possible for the zonal-mean method in z-space to misattribute heat transport by the gyre to the overturning, as illustrated in the lower panel

221

222

Thought experiment A: no gyre, and upper western boundary current is warm Americas Europe Zonal average of temperature and zonal integral of velocity Small heat transport by overturning

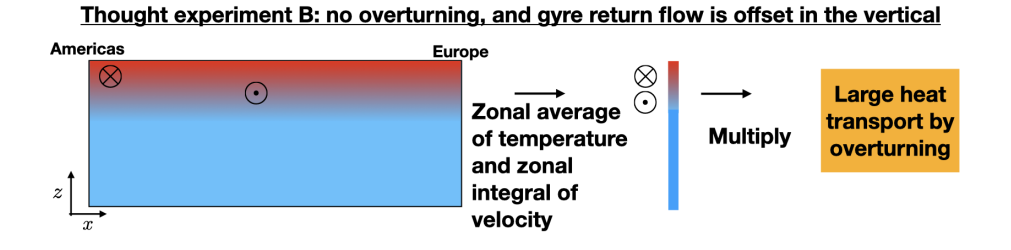


Figure 2. Two thought experiments that illustrate potential problems with the zonal-mean method in z-space. Thought experiment A shows a scenario where there is no gyre, but the northward flowing western boundary current is much warmer than the rest of the basin. Hence when a zonal mean is taken, the temperature associated with northward flowing water is lower than the actual temperature of the water that is flowing north, and the heat transport associated with overturning is small, leaving a large heat transport by the gyre. Thought experiment B shows a scenario where there is no overturning transport, but because the gyre return flow occurs at a different depth from the gyre's western boundary current, the heat transport is attributed to overturning.

of figure 2: in this case the northward and southward flowing parts of the gyre are offset in the vertical, so some of its heat transport is attributed to overturning.

2.1.3 The Talley03 method

223

224

225

226

227

228

229

230

Talley (2003) developed a method for splitting the heat transport in the subtropical gyre into the heat transport by the overturning and the heat transport by the gyre. At the latitudes of the Northern Hemisphere subtropical gyres, northward-flowing AMOC transport is assumed to follow the western boundary, but to have a higher density than the northward-flowing transport associated with the gyre itself. Talley (2003) considers

the heat transport due to the Ekman transport separately, but here we include it in the heat transport due to the gyre.

First, the isopycnal that defines the bottom of the subtropical gyre is chosen. Here we call this isopycnal ρ_{int} , because it represents the bottom of the gyre in the ocean interior. This isopycnal is shown by the magenta line in figure S1. The velocity field is integrated in the vertical above this isopycnal. In the west of the basin, this depth-integrated velocity is northward, and in the rest of the basin it is southward: the longitude that splits these two regions, x_{tal} is found. The total southward volume transport of the gyre ψ_{gyre} is defined to be the total transport east of x_{tal} and above the isopycnal ρ_{int} , so

$$\psi_{gyre} = \int_{x_{tot}}^{x_e} \int_{-H}^{0} v_{vc} \mathcal{H}(\rho - \rho_{int}) dz dx, \qquad (9)$$

where $\mathcal{H}(\rho - \rho')$ is a step function that is one above ρ' and zero below ρ' .

The total northward volume transport of the gyre must be defined to be equal to the total southward volume transport of the gyre. To achieve this, we define the isopycnal ρ_{west} such that the total volume transport west of x_{tal} and above ρ_{west} is equal to the total transport ψ_{qyre} . Hence the total heat transport by the gyre is defined to be

$$OHT_{gyre}^{(tal)}(t) = \int_{-H}^{0} \int_{x_{w}}^{x_{tal}} v_{vc} \theta \mathcal{H}(\rho - \rho_{west}) \, dz \, dx + \int_{-H}^{0} \int_{x_{tal}}^{x_{e}} v_{vc} \theta \mathcal{H}(\rho - \rho_{int}) \, dz \, dx \,. \quad (10)$$

The heat transport associated with the overturning is the integral of the heat transport over the rest of the ocean.

This method avoids the pitfalls of the zonal-mean methods, and takes into account physical information about the overturning circulation, which tends to follow the west-ern boundary. Higher-density waters are more likely to continue into the subpolar North Atlantic without recirculating in the subtropical gyre (Berglund et al., 2022). This method associates these higher density waters with AMOC. However, it only applies in the subtropical gyres on the Northern Hemisphere, and cannot easily be extended outside these latitudes. Talley herself modifies the method substantially to apply it in other regions.

In this manuscript, we apply the Talley (2003) method to the meridional velocity field after performing a 24-month rolling time average in density space. Without this time average, x_{tal} moves around a lot and ρ_{west} is not always well-defined.

2.1.4 The streamfunction-splitting method

Our new method has similarities to the Talley (2003) method, but instead of associating higher densities with AMOC, our method associates water at a particular range of longitudes with AMOC. This is motivated by the pathway of water in the northward limb of the AMOC, as illustrated by the pseudo-streamfunction (C. Jones & Cessi, 2018), which is plotted in the bottom panel figure 3,

$$\Phi = \int_{x_m}^x \int_{-H}^0 v \mathcal{H}(\rho - \rho_m) \, \mathrm{d}z \, \mathrm{d}x' \,, \tag{11}$$

where \mathcal{H} is the Heaviside function and ρ_m is the isopycnal that passes through the maximum of the meridional overturning streamfunction (the yellow dashed-dotted line in figure 3). This isopycnal is chosen because the net transport is northward above the isopycnal and southward below the isopycnal, ensuring that the total northward AMOC transport is included in the pseudostreamfunction.

As shown in the bottom panel of figure 3, the AMOC's northward branch winds around the gyres, following the red contours northward. The blue contours in figure 3 represent the gyres. We expect that the strength of the gyres is independent of the strength of AMOC at long timescales, and that the gyres are primarily driven by the wind, although recirculation of northward AMOC transport may also be present.

Of course, in reality some water parcels that start in on the red streamlines will enter the blue region and vice-versa, both because of mixing and because water is exchanged across streamlines by vertically sheared flows. The red streamlines are not supposed to represent a "conveyor belt" pathway, but simply a pathway where flow is generally continuing northward as part of AMOC.

Because the circulation is three-dimensional, the total transport above density surface ρ_m contains a small divergent component, and Φ is not a traditional streamfunction. A small number of open contours like the purple contour in figure 3 do not originate in the far south. These contours represent the movement of water that upwelled across ρ_m within the domain.

In general, the red contours that represent the AMOC occupy the western boundary only at latitudes with clockwise gyre circulation. In this paper, we focus on these latitudes, because the AMOC pathway does not move around very much at these latitudes. We plan to extend the method to other latitudes in future.

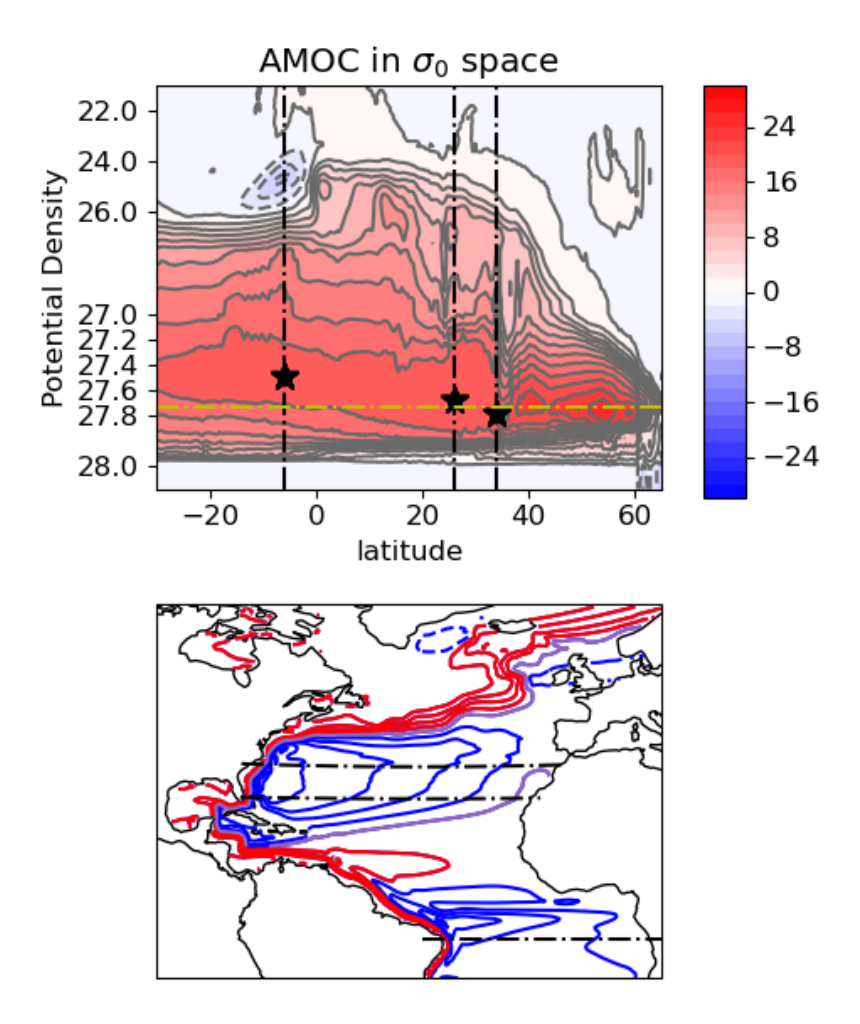


Figure 3. (Top) The Atlantic Meridional Overturning Circulation in potential density space. The black vertical dashed-dotted lines indicate the three latitudes where the methods are applied and the stars indicate the local AMOC maximum at each latitude. (Bottom) The red, blue and purple contours in the left panel show the pseudostreamfunction, the mean transport above $\sigma_0 = 27.74$ (an isopycnal that passes through the maximum MOC streamfunction, as shown by the horizontal yellow line in figure 3a) integrated from the western boundary eastward. The contour interval is 5 Sv. Red contours are contours that start in the south and end in the north, representing the AMOC. Blue contours are coutours that cross each latitude twice, representing the gyres. The purple contour represents water that upwells across isopycnal ρ_m : at latitudes where the contour appears twice, this flow is part of the gyre, and at latitudes where this contour appears once this flow is par of AMOC. The black dashed-dotted lines show the three latitudes used in this study.

In our new method, which we call the streamfunction splitting method, a constantlatitude section is divided into three regions. The first region is the deep region: this region is defined as the area below the dividing isopycnal, the green region with southward flow in the bottom panel of figure 1. This dividing isopycnal is chosen to be the isopycnal that passes through the maximum of the meridional overturning streamfunction at that latitude (see stars in figure 3a). The net transport above this isopycnal is northward and the net transport below it is southward, and this choice of dividing isopycnal is below the depth of the gyres at all latitudes in the Atlantic. The second region is the western-boundary region, the green region with northward flow in the bottom panel of figure 1, which is defined as the region above the dividing isopycnal and west of the latitude x^* . Latitude x^* is chosen such that the volume transport through the deep (green southward) region plus the volume transport through the western boundary (green northward) region sums to zero. The third region is the gyre region, the light blue region in the bottom panel of figure 1, and this region is defined to be above the dividing isopycnal and east of x^* . By definition, the volume transport through the gyre region is zero. The heat transport by the overturning is defined as the heat transport through the deep region plus the heat transport through the western boundary region. The heat transport by the gyre is defined as the heat transport through the gyre region.

Here, we apply this streamfunction splitting method to the meridional velocity field after performing a 24-month rolling time average in density space. Without this time-average, x^* moves around a lot and sometimes is not defined. Note that x^* is close to the western boundary in all cases, meaning that there is strong northward flow in the western boundary current that is associated with AMOC.

3 Results

287

288

289

290

291

292

293

294

297

298

299

300

301

302

303

305

309

310

311

312

313

314

315

316

317

3.1 Time-mean heat transport by the gyres vs. overturning

The time-mean heat transport in each method is shown in Table 1. The time-mean heat transport attributed to AMOC varies with latitude and with the method used, but it is very similar between ensemble members.

At 34 °N and 26 °N, the z-space method attributes almost all the heat transport to overturning, whereas at 5 °S, the z-space method only attributes about 65% of heat transport to overturning, meaning that according to the z-space method the net trans-

Table 1. Proportion of time and ensemble-mean heat transport associated with AMOC in each method, together with the standard deviation between ensemble members.

Latitude	34 °N	26 °N	5 °S
z-space method	$91.5 \pm 0.5\%$	$99.6 \pm 0.3\%$	$65.4\pm0.1\%$
Density-space method	$115.1\pm0.3\%$	$117.8\pm0.3\%$	$108.5\pm0.1\%$
Talley03 method	$69.3\pm0.2\%$	$66.8\pm0.1\%$	N/A
Streamfunction-splitting method	$102.7\pm0.2\%$	$96.5\pm0.2\%$	$143.7\pm0.3\%$

port of the tropical gyre at 5 °S is northward. The z-space method is the only method that attributes a mean northward heat transport to the tropical gyre at 5 °S. While gyres can transport heat upgradient, the authors can think of no reason why the South Atlantic tropical gyre should do so. The subtropical cell is primarily a vertical circulation that comprises poleward flow very close to the surface and equatorward flow in the top 100m or so of the water column: because of the strong temperature contrast between these two parts of the flow, the subtropical cell transports a lot of heat. But even if the heat transport of the subtropical cell is counted as overturning, there is no reason for the remainder of the heat transport by the gyre to be northward. It is possible that at this latitude, the zonal-mean method in z-space has one of the problems illustrated in figure 2.

The Talley method indicates that about 69% of heat transport is carried by the overturning at 34 °N, with 67% carried by the overturning at 26 °N. The Talley method yields lower estimates than the other methods, because it associates the upper layer of water with the gyre, and this upper layer of water performs a significant fraction of the northward heat transport, consistent with the Talley (2003) estimate that the gyre carries 0.1-0.3 PW of heat out of a total heat transport of 1.4 PW at 24 °N.

At all three latitudes, the density-space method attributes more than 100% of the northward heat transport to AMOC, meaning that the gyre transports heat southward. As shown in figure S2, at 34 °N and 26 °N the southward transport in the gyre is warmer than the northward transport in the western boundary current when density is held constant. The size of this compensation is much larger in the density space method than in the streamfunction splitting method. One possible reason is that significant density

change occurs as water flows around the gyre, and in the density-space method any water that experiences density change is counted as overturning. This is a version of the situations is described in Figure 2, Thought experiment B. This highlights that the main assumption of the density space method is that the gyres follow isopycnal surfaces: this assumption may not be a valid.

The streamfunction-splitting method also attributes more than 100% of the total mean heat transport to AMOC, indicating that the subtropical gyre transports heat southward at 34°N. It is sometimes claimed that the gyres always transport heat down-gradient, but given the significant exchange of water between the warm northward-flowing AMOC flow and the subtropical gyre in the Gulf Stream and Gulf Stream extension region (Berglund et al., 2022), a small southward heat transport by the subtropical gyre is physically plausible.

At 26 °N, the streamfunction-splitting method attributes about 97% of heat transport to the overturning, which is in agreement with the z-space method. At 5°S, the streamfunction-splitting method attributes nearly 150% of the heat transport to overturning. In other words this method attributes more southwater heat transport to the tropical gyre than either of the other methods. It makes sense that the gyre should transport heat downgradient (southward) at this latitude.

One reason why the zonal-mean method in z-space and the streamfunction splitting method give such different results is that the zonal-mean method in z-space counts the subtropical cell in the overturning transport. The subtropical cell is primarily a vertical circulation that comprises poleward flow very close to the surface and equatorward flow in the top 100m or so of the water column: because of the strong temperature contrast between these two parts of the flow, the subtropical cell transports a lot of heat. The streamfunction splitting method counts the most of the subtropical cell in the gyre transport, because it takes place away from the western boundary.

3.2 Heat transport variability in the CESM large ensemble

Before applying each of the methods to heat transport variability, it is helpful to look at the correlation between AMOC and Ocean Heat Transport at the three different latutdes discussed above. Figure 4a-c shows the timeseries of heat and AMOC transport at the three chosen latitudes for the third ensemble member, which is chosen as a

representative ensemble member. Heat transport is strongly correlated with AMOC at all three latitudes and for both timescales of variability shown here (orange and blue lines in 4a-c). Figure 4d-e shows the correlation between AMOC transport and heat transport at the three chosen latitudes for all ensemble members, plotted as a function of the standard deviation of AMOC strength. Both AMOC variability and its correlation with heat transport are stronger at 34°N and 26°N than at 5°S on 2-10yr timescales (figure 4d) and on 10+yr timescales (figure 4e). Most ensemble members show stronger correlations between AMOC and heat transport at 10+yr timescales than at 2-10yr timescales, consistent with the idea that wind-driven gyre variability is averaged out on timescales larger than 10 years.

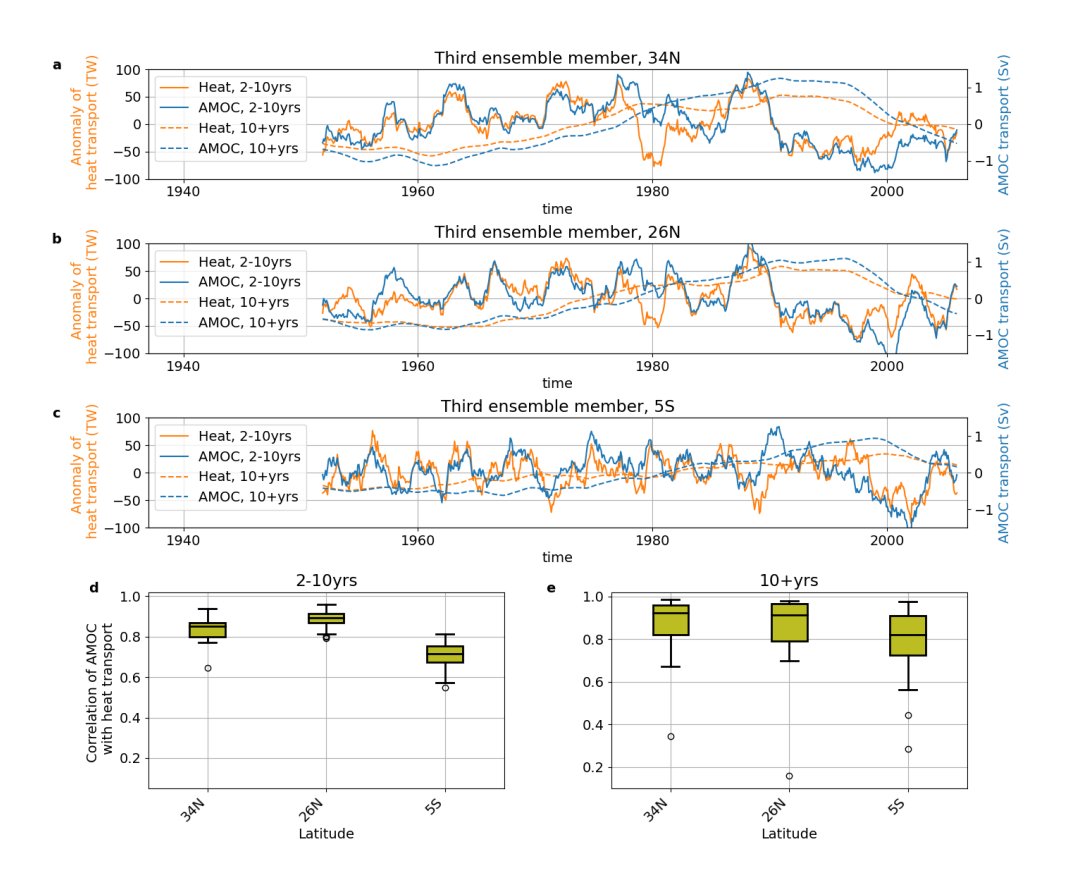


Figure 4. Timeseries of AMOC transport (blue) and heat transport (orange) for the third ensemble member, filtered to pick out variability on 2-10yr timescales (solid lines) and 10+yr timescales (dashed lines) at a) 34°N, b) 26°N and c) 5°S. The correlation between the smoothed heat transport and the smoothed AMOC transport at 34°N, 26°N and 5°S, filtered to pick out variability on d) 2-10yr timescales and e) 10+yr timescales (dashed lines). Open circles indicate outliers.

Given the strong correlation between AMOC and OHT, we expect that AMOC is the strongest driver of variability at all three latitudes. The remainder of this work aims to elucidate the controls on heat transport at these different latitudes and to compare methods for separating northward heat transport by the gyres from northward heat transport by the overturning circulation.

3.3 Time-varying heat transport by the gyres vs. overturning

Next, we separated the heat transport variability into variability attributed to the gyres and variability attributed to the AMOC using the four methods described in section 2. Using a running mean that is applied after the heat transport is partitioned into heat transport by the overturning and heat transport by the gyres, we further separate the heat transport variability into variability on 2-10yr timescales and variability on 10+year timescales. Ten years is chosen for ease of comparison with previous studies (e.g. Larson et al. (2020)). The results are plotted in figure 5.

3.3.1 Heat transport variability in the North Atlantic subtropical gyre

In most ensemble members, at 34°N and 26°N all methods attribute about 80-100% of the heat transport variability to the overturning at 2-10 yr timescales (figure 5a and e), meaning that the gyre is responsible for 0-20% of the heat transport variability. The Talley method attributes slightly less heat transport to AMOC than the other three methods.

At multidecadal timescales (figure 5b and d) there is more disagreement between methods. Again the Talley method produces the lowest estimate, with about 80% of 10+ yr heat transport variability attributed to AMOC at 26° N.

The zonal-mean method in density space attributes slightly more than 100% of the heat transport variability to the overturning on 10+yr timescales. Our new method, which we call the streamfunction splitting method, attributes about 110-120% of the heat transport variability to the overturning on 10+yr timescales. More heat transport is attributed to AMOC than one might expect based on the correlation between AMOC transport and the total heat transport. The extra variability is compensated by heat transport attributed to the gyre, which is anti-correlated with AMOC transport at 10+yr timescales. When compensation occurs in the zonal-mean methods, it is difficult to understand what is caus-

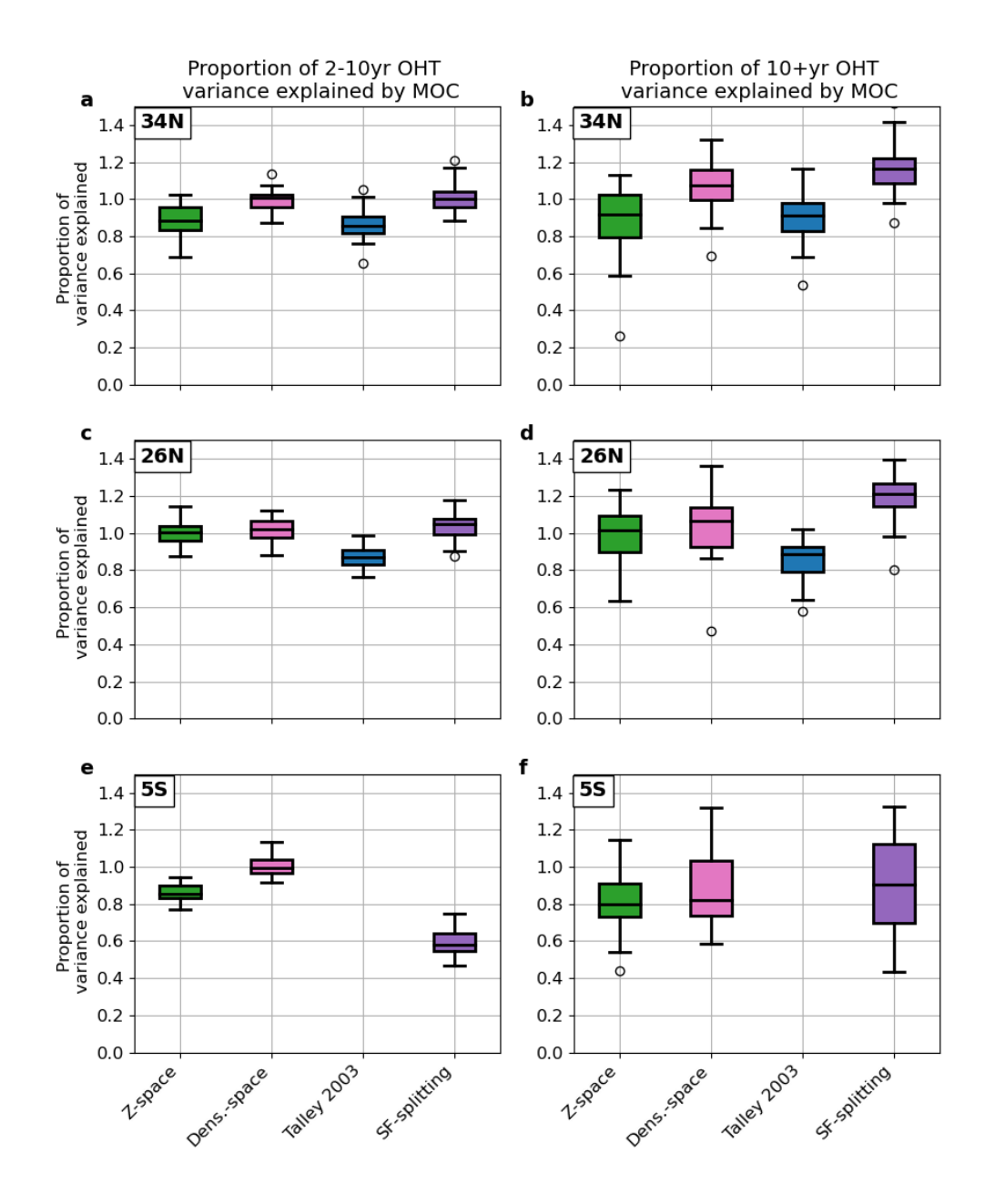


Figure 5. A box and whisker plot of the heat transport variability on 2-10 yr timescales explained by each method at a) 34 °N, c) 26 °N, and e) 5°S, and on 10+ yr timescales at b) 34 °N, d) 26 °N, and f) 5°S, where the green box represents the proportion of variance explained by AMOC for the zonal-mean method in z space, the pink box represents the proportion of variance explained by AMOC for the zonal-mean method in density space, and the blue box represents the variance explained by AMOC for the Talley 2003 method and the purple box represents the variance explained by AMOC for the streamfunction-splitting method. Open circles indicate outliers.

ing this compensation, but in the streamfunction splitting method it is very clear. Times with high heat transport in the western boundary are associated with times of low heat transport in the gyre region and vice versa. This can easily be explained: when the AMOC transport is larger, more heat is transported northward and temperatures north of 26°N increase, reducing the difference in temperature between northward and southward flowing water in the gyre region. At the same time, temperatures in the western boundary decrease. Hence, when the AMOC transports more heat northward on the western boundary, the gyre transports less heat back southward. This is illustrated in figure 6, which shows the mean temperature in the top 400m over all time slices where the low-pass filtered AMOC strength is greater than average minus the mean temperature over the top 400m for all time slices.

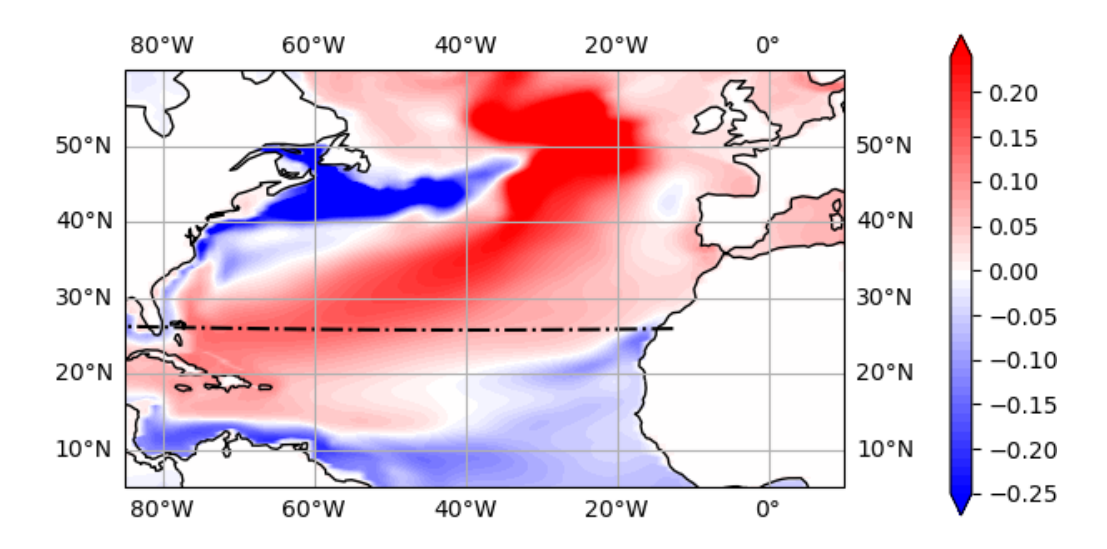


Figure 6. The mean temperature in the top 400m over all time slices where the low-pass filtered AMOC strength is greater than the mean AMOC strength minus the mean temperature over the top 400m for all time slices.

Because 26°N and 34°N are close together and both occur in the subtropical gyre, we expect that heat transport by the overturning at 26°N and at 34°N are similar to each other, particularly at long timescales. In figure 7, we plot the correlation between the heat transport by the overturning at 26°N and at 34°N for the 2-10yr timescale and for the 10+yr timescale. The zonal-mean method in density space, the Talley method, and the streamfunction splitting method all find strong correlations between ocean heat transport attributed to overturning at 26°N and at 34°N, while the zonal-mean method in

z-space generally finds weaker correlations between the two latitudes. This is particularly obvious at 10+yr timescales, for which the correlation between 26°N and at 34°N is close to one for the streamfunction splitting method. These results suggest that the zonal-mean method in z-space is less robust than the other three methods, and may give different results even at similar latitudes.

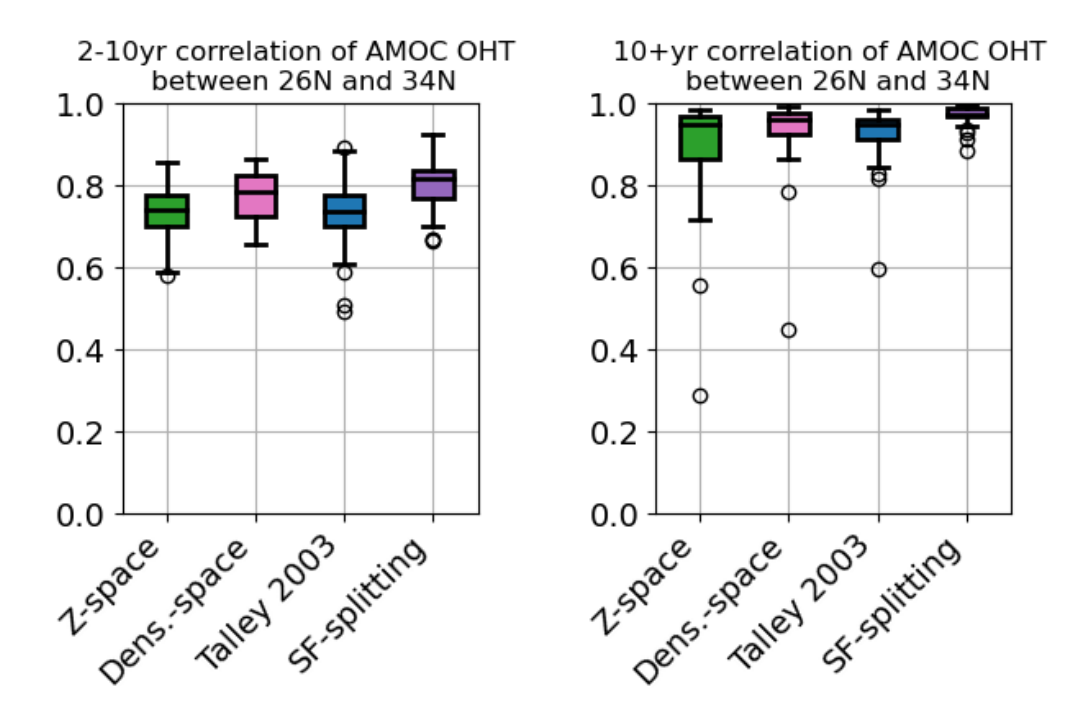


Figure 7. The left panel shows box and whisker plots of the correlation between the ocean heat transport attributed to AMOC at 26°N and at 34°N for each ensemble member, filtered to select 2-10yr timescales. The right panel shows the same, but filtered to select 10+ yr timescales. For the green box, OHT attributed to AMOC is calculated using the zonal-mean method in z-space, for the pink box OHT attributed to AMOC is calculated using the zonal-mean method in density space, and for the blue box OHT attributed to AMOC is calculated using the Taley 2003 method, andfot he purple box OHT attributed to AMOC is calculated using the streanfunction-splitting method. Open circles indicate outliers.

3.3.2 Heat transport variability in the North Atlantic subtropical gyre

At 5° S, the zonal-mean method in z-space attributes about 85% of the heat transport variability to AMOC on 2-10yr timescales (figure 5e). The zonal-mean method in

density space attributes about 100% of the heat transport variability to AMOC, with no role for gyres in the variability. The streamfunction splitting method attributes about 55% of 2-10yr heat transport variability to AMOC. At 5°S, the subtropical cell comprises southward flow near the surface and northward flow at depth, as shown in figure S1c. As discussed above, the zonal-mean method in z-space counts the subtropical cell in the overturning transport, whereas the streamfunction-splitting method does not. As a result a higher proportion of short-timescale variability is attributed to AMOC in the z-space method than in the streamfunction-splitting method.

At 10+yr timescales, the zonal-mean method in z-space and the streamfunction-splitting method estimate that about 80% of heat transport variability is attributed to the overturning (figure 5f). The variability of the subtropical cell generally has much shorter timescales, so it is not an important source of multidecadal variability.

4 Conclusions

In this paper, we present four methods for partitioning the AMOC heat transport and the gyre heat transport in the Atlantic basin. The first two methods estimate the heat transport by the AMOC using the product of the zonal-mean temperature and the zonally-integrated volume transport. The first method takes the zonal mean and zonal integral in depth space: we call this method the zonal-mean method in z-space. The second method takes the zonal mean and zonal integral in density space: we call this method the zonal-mean method in density-space. The third and fourth method leverage physical insights about the flow pathway. The third method, adapted from Talley (2003), works only in the subtropical gyre, using the assumption that AMOC waters follow the western boundary and are confined to deeper isopycnals. The fourth method is a new method that does not assume anything about the density of the flow, but instead assumes that the flow follows the pseudostreamfunction pathway shown in figure 3. We call this method the streamfunction splitting method.

We compare the methods at three different latitudes: $34^{\circ}N$, $26^{\circ}N$ and $5^{\circ}S$. The proportion of the time-mean heat transport attributed to AMOC is significantly different between methods. At 34 °N and $26^{\circ}N$, the z-space method and the streamfunction splitting method both attribute about 100% of time-mean heat transport to AMOC, but the density-space method attributes about 115% of heat transport to AMOC, because on

isopycnals the southward transport is warmer than the northward transport. The Talley method only attributes about 70% of time-mean heat transport to the overturning at these latitudes. At 5°S, there is even more disagreement between methods, and the streamfunction-splitting method attributes about 140% of the time-mean heat transport to AMOC, significantly more than the other two methods.

We then turn to the heat transport variability. All methods agree that about 80-100% of heat transport variability on 2-10yr timescales is attributed to AMOC at 34° N and at 26° N, with little compensation between the heat transport by the AMOC and the heat transport by the gyres. Estimates of the proportion of multidecadal heat transport variability carried by the AMOC are sensitive to method choice. The zonal-mean method in z-space and the Talley method give lower values for the heat transport variability due to AMOC than the other methods.

At 34°N and at 26°N, the Talley method attributes the lowest fraction of the heat transport (about 80%) and heat transport variability to AMOC and our new method attributes the highest fraction of the heat transport variability to AMOC (about 110%). Each of these two methods makes an imperfect assumption about the location of AMOC transport, with the Talley method assuming AMOC transport follows denser isoycnals and the streamfunction splitting method assuming AMOC transport follows the western boundary. The real transport is likely to be somewhere between the two methods. As a result, the Talley method and the streamfunction-splitting method could be taken to represent the upper and lower bounds on the fraction of heat transport variability attributed to AMOC.

At 5°S, the subtropical cell contributes to the vertical part of the meridional heat transport, but may or may not be considered part of the AMOC. Both the zonal-mean method in z-space and the streamfunction-splitting method are somewhat informative at this latitude: their differences highlight that much of the subtropical cell is found outside the western boundary, and that the subtropical cell is a significant cause of heat transport variability on 2-10yr timescales.

All of the methods presented here have advantages and disadvantages. Some of these are listed below:

- The zonal-mean method in z-space is the easiest method to apply to observations, because the total volume transport on a depth level can be estimated from a small number of measurements at each side of the basin. However, this method is susceptible to the problems illustrated in figure 2.
- The zonal-mean method in density-space takes into account that the AMOC is usually defined in density coordinates. But this method is also susceptible to the problems illustrated in figure 2.
- The Talley method makes physically well-justified assumptions in the subtropical gyre, and its components could be further decomposed to understand the causes of variability in the AMOC and gyre regions. For example, it would be easy to determine the zonal mean temperature in the northward-flowing AMOC is correlated or anti-correlated with AMOC strength and to examine how this contributes to the heat transport by the overturning. However, it cannot be applied outside the subtropical gyre without significant adaptations.
- The streamfunction-splitting method also makes physically-motivated assumptions, and its components could be further decomposed to understand the causes of variability in the AMOC and gyre regions. At the moment it can only be applied in the Atlantic at latitudes where the gyre is clockwise. However we plan to improve the method to work at all latitudes in the future.

This paper focuses on partitioning heat transport in model output. While we have applied these methods to a coarse-resolution ocean model, they could easily be applied to an eddying ocean model, and we hope to do this in the future.

5 Open Research

The code repository for this paper is at https://zenodo.org/doi/10.5281/zenodo.11283728 (C. S. Jones, 2024). The data used in this research is the CESM1 Large Ensemble, which is hosted on Amazon Web Services (de La Beaujardiere et al., 2019). This work would not have been possible without the tools provided by and maintained by the Pangeo community (https://pangeo.io/).

Acknowledgments

- 528 Thanks to Navid Constantinou, Paola Cessi and Ian Eisenmann for useful discussions
- about this work. CSJ's work on this project was supported by NSF award number OCE-
- ₅₃₀ 2219852.

527

531

References

- Berglund, S., Döös, K., Groeskamp, S., & McDougall, T. J. (2022). The downward spiralling nature of the north atlantic subtropical gyre. *Nature communi*-
- cations, 13(1), 2000.
- Bhagtani, D., Hogg, A. M., Holmes, R. M., & Constantinou, N. C. (2023). Surface
- heating steers planetary-scale ocean circulation. Journal of Physical Oceanog-
- raphy.
- Boccaletti, G., Ferrari, R., Adcroft, A., Ferreira, D., & Marshall, J. (2005). The ver-
- tical structure of ocean heat transport. Geophysical Research Letters, 32(10).
- Borchert, L. F., Müller, W. A., & Baehr, J. (2018). Atlantic ocean heat transport
- influences interannual-to-decadal surface temperature predictability in the
- north atlantic region. Journal of Climate, 31(17), 6763–6782.
- Bryan, K. (1962). Measurements of meridional heat transport by ocean currents.
- Journal of Geophysical Research, 67(9), 3403–3414.
- Buckley, M. W., & Marshall, J. (2016). Observations, inferences, and mechanisms
- of the Atlantic Meridional Overturning Circulation: A review. Reviews of Geo-
- physics, 54(1), 5-63.
- ⁵⁴⁸ Cessi, P. (2018). The effect of Northern Hemisphere winds on the meridional over-
- turning circulation and stratification. Journal of Physical Oceanography,
- 48(10), 2495-2506.
- de La Beaujardiere, J., Banihirwe, A., Shih, C., Paul, K., & Hamman, J. (2019).
- NCAR CESM LENS cloud-optimized subset [Dataset]. UCAR/NCAR Compu-
- tational and Informations Systems Lab. doi: 10.26024/wt24-5j82
- Eden, C., & Willebrand, J. (2001). Mechanism of interannual to decadal variability
- of the North Atlantic circulation. Journal of Climate, 14(10), 2266–2280.
- Ferrari, R., & Ferreira, D. (2011). What processes drive the ocean heat transport?
- Ocean Modelling, 38(3-4), 171–186.
- Folland, C. K., Palmer, T. N., & Parker, D. E. (1986). Sahel rainfall and worldwide

- sea temperatures, 1901-85. Nature, 320(6063), 602-607.
- Foukal, N. P., & Chafik, L. (2022). The AMOC needs a universally-accepted definition. Authorea Preprints.
- Goldenberg, S. B., Landsea, C. W., Mestas-Nuñez, A. M., & Gray, W. M. (2001).

 The recent increase in Atlantic hurricane activity: Causes and implications.
- Science, 293(5529), 474–479.
- Gray, A. R., & Riser, S. C. (2014). A global analysis of Sverdrup balance using
 absolute geostrophic velocities from Argo. Journal of Physical Oceanography,
 44(4), 1213–1229.
- Hall, M. M., & Bryden, H. L. (1982). Direct estimates and mechanisms of ocean heat transport. Deep Sea Research Part A. Oceanographic Research Papers, 29(3), 339–359.
- Jackson, L., Kahana, R., Graham, T., Ringer, M., Woollings, T., Mecking, J., & Wood, R. (2015). Global and European climate impacts of a slowdown of the AMOC in a high resolution GCM. Climate dynamics, 45, 3299–3316.
- Jones, C., & Cessi, P. (2018). Components of upper-ocean salt transport by the gyres and the meridional overturning circulation. *Journal of Physical Oceanog*raphy, 48(10), 2445–2456.
- Jones, C. S. (2024). cspencerjones/amoc_heat_code: Plots for Jones et al. 2024 (2nd submission) [software]. Zenodo. doi: 10.5281/zenodo.11283729
- Kang, S. M., Frierson, D. M., & Held, I. M. (2009). The tropical response to extratropical thermal forcing in an idealized GCM: The importance of radiative feedbacks and convective parameterization. *Journal of the atmospheric sciences*, 66(9), 2812–2827.
- Kay, J. E., Deser, C., Phillips, A., Mai, A., Hannay, C., Strand, G., . . . others

 (2015). The Community Earth System Model (CESM) large ensemble project:

 A community resource for studying climate change in the presence of internal

 climate variability. Bulletin of the American Meteorological Society, 96(8),

 1333–1349.
- Klotzbach, P., Gray, W., & Fogarty, C. (2015). Active Atlantic hurricane era at its end? *Nature Geoscience*, 8(10), 737–738.
- Larson, S. M., Buckley, M. W., & Clement, A. C. (2020). Extracting the buoyancydriven Atlantic meridional overturning circulation. *Journal of Climate*, 33(11),

- 592 4697-4714.
- Marshall, J., Donohoe, A., Ferreira, D., & McGee, D. (2014). The ocean's role in setting the mean position of the Inter-Tropical Convergence Zone. Climate Dy-
- namics, 42, 1967-1979.
- Martin, E. R., & Thorncroft, C. D. (2014). The impact of the AMO on the West
- African monsoon annual cycle. Quarterly Journal of the Royal Meteorological
- Society, 140(678), 31–46.
- McDonagh, E. L., McLeod, P., King, B. A., Bryden, H. L., & Valdés, S. T. (2010).
- 600 Circulation, heat, and freshwater transport at 36 N in the Atlantic. Journal of
- physical oceanography, 40(12), 2661–2678.
- Oldenburg, D., Wills, R. C., Armour, K. C., Thompson, L., & Jackson, L. C. (2021).
- Mechanisms of low-frequency variability in North Atlantic Ocean heat trans-
- port and AMOC. Journal of Climate, 34(12), 4733–4755.
- Pickart, R. S., & Spall, M. A. (2007). Impact of Labrador Sea convection on
- the North Atlantic meridional overturning circulation. Journal of Physical
- Oceanography, 37(9), 2207–2227.
- Piecuch, C. G., Ponte, R. M., Little, C. M., Buckley, M. W., & Fukumori, I. (2017).
- Mechanisms underlying recent decadal changes in subpolar North Alantic
- Ocean heat content. Journal of Geophysical Research: Oceans, 122(9), 7181-
- ₆₁₁ 7197.
- Roemmich, D., & Wunsch, C. (1985). Two transatlantic sections: Meridional circula-
- tion and heat flux in the subtropical North Atlantic Ocean. Deep Sea Research
- Part A. Oceanographic Research Papers, 32(6), 619–664.
- Rypina, I. I., Pratt, L. J., & Lozier, M. S. (2011). Near-surface transport pathways
- in the North Atlantic Ocean: Looking for throughput from the subtropical to
- the subpolar gyre. Journal of Physical Oceanography, 41(5), 911–925.
- Stommel, H. (1957). A survey of ocean current theory. Deep Sea Research (1953), 4,
- 149–184.
- Talley, L. D. (1999). Some aspects of ocean heat transport by the shallow, inter-
- mediate and deep overturning circulations. Geophysical Monograph-American
- $Geophysical\ Union,\ 112,\ 1-22.$
- Talley, L. D. (2003). Shallow, intermediate, and deep overturning components of the
- global heat budget. Journal of Physical oceanography, 33(3), 530–560.

- Trenberth, K. E., & Fasullo, J. T. (2017). Atlantic meridional heat transports computed from balancing earth's energy locally. Geophysical Research Letters,

 44(4), 1919–1927.
- Warren, B. A. (1999). Approximating the energy transport across oceanic sections.

 Journal of Geophysical Research: Oceans, 104(C4), 7915–7919.
- Yan, X., Zhang, R., & Knutson, T. R. (2018). Underestimated AMOC variability and implications for AMV and predictability in CMIP models. *Geophysical Research Letters*, 45(9), 4319–4328.
- Yang, H., Li, Q., Wang, K., Sun, Y., & Sun, D. (2015). Decomposing the meridional heat transport in the climate system. *Climate Dynamics*, 44, 2751–2768.
- Yang, J. (2015). Local and remote wind stress forcing of the seasonal variability of
 the Atlantic Meridional Overturning Circulation (AMOC) transport at 26.5 N.

 Journal of Geophysical Research: Oceans, 120(4), 2488–2503.
- Yeager, S. G., Karspeck, A. R., & Danabasoglu, G. (2015). Predicted slowdown in the rate of Atlantic sea ice loss. *Geophysical Research Letters*, 42(24), 10–704.
- Young, W. R. (2012). An exact thickness-weighted average formulation of the Boussinesq equations. *Journal of Physical Oceanography*, 42(5), 692–707.
- Zhang, R., Sutton, R., Danabasoglu, G., Kwon, Y.-O., Marsh, R., Yeager, S. G., ...

 Little, C. M. (2019). A review of the role of the Atlantic meridional overturning circulation in Atlantic multidecadal variability and associated climate
 impacts. Reviews of Geophysics, 57(2), 316–375.
- Zhang, R., & Thomas, M. (2021). Horizontal circulation across density surfaces
 contributes substantially to the long-term mean northern Atlantic Meridional
 Overturning Circulation. Communications Earth & Environment, 2(1), 112.